Two-fluid-model analysis of low-temperature thermodynamic data for Si:P

C. Kasl and M. J. R. Hoch
Department of Physics, University of the Witwatersrand, P.O. Wits 2050, South Africa
(Received 12 January 1998)

A detailed analysis of available low-temperature ($T \lesssim 1$ K) thermodynamic response-function data for Si:P in the vicinity of the metal-insulator transition has been carried out using a two-fluid model which allows for both localized and itinerant electron contributions. This analysis provides information on the relative concentration of the two electron ''fluids'' as a function of the concentration through the critical region. The specific-heat data, in both zero and nonzero magnetic fields, is successfully described in terms of this two-fluid model. [S0163-1829(98)00724-3]

I. INTRODUCTION

A large body of experimental information on the transport and thermodynamic properties of metal-insulator (MI) systems has been obtained over the years. A variety of theoretical approaches has been developed in order to understand and explain the observations. A recent review[1] gives an account of these efforts with emphasis on field theory methods.

For heavily doped semiconductors such as Si:P, measurements of thermodynamic response functions, including the magnetic susceptibility and specific heat, have been extended to lower temperatures and a wider range of magnetic fields than previously. In a previous paper[2] we have given a preliminary account of the analysis of some of these results using a two-fluid model involving localized and itinerant electrons. Our work has built on the approaches of Bhatt and Lee[3] and Sarachik *et al.*[4] for the magnetic susceptibility of insulating material, incorporating interacting spins, and the later work of Paalanen *et al.*[5] for the specific heat and susceptibility of insulating and just-metallic samples. We introduced an extension of the two-fluid model to finite magnetic fields, and also showed that these equations can explain available experimental data in high magnetic fields.

While the model is phenomenological and cannot predict the proportions of localized and itinerant electrons for a given dopant concentration near the critical concentration n_c, it has the virtue of explaining a large number of experimental observations in a consistent way. Lakner *et al.*[6] have also given a description of the local moment concentration in the metallic phase. By introducing a distribution of Kondo temperatures, they show that the Kondo effect can explain the power-law behavior observed in the zero-field specific heat for $n \sim n_c$.

In this paper we give a more detailed account of the application of the two-fluid model to experimental results obtained in high magnetic fields and at comparatively low temperatures below 1 K. We also present an analysis of zero-field specific-heat data. Information on the relative concentrations of localized and itinerant electrons through the critical region is obtained.

II. THE TWO-FLUID MODEL

In nonzero magnetic fields ($B \neq 0$) the two-fluid-model equations[2] for the specific-heat coefficient γ and the susceptibility χ may be written in the form

$$\frac{\gamma}{\gamma_0} = \frac{m^*}{m_0^*} + \delta(y)\left(\frac{T}{T_0}\right)^{-\alpha}, \tag{1}$$

$$\frac{\chi}{\chi_0} = \frac{m^*}{m_0^*} + \varepsilon(y)\left(\frac{T}{T_0}\right)^{-\alpha}, \tag{2}$$

where $\delta(y)$ and $\varepsilon(y)$ are functions of $y = g\mu_B B/k_B T$, and are evaluated by numerical integration. The quantity α is the exponent in the renormalized exchange coupling distribution $P(J) \sim J^{-\alpha}$. γ_0 and χ_0 are Fermi-liquid values for the specific-heat coefficient and the magnetic susceptibility, respectively, while m^* is the Fermi-liquid effective mass of the impurity itinerant electrons and $m_0^* = 0.34 m_0$ is the Si conduction-band mass. T_0 is a parameter which depends on the fraction of localized moments.

The forms of the factors $\delta(y)$ and $\varepsilon(y)$ are shown in Fig. 1, plotted as a function of $1/y$. For this plot these terms have been evaluated numerically for $\alpha = 0.6$, which is a value found[5] close to the MI transition. For large y (high B/T), δ and ε have an asymptotic form $y^{-\alpha}$, which implies that both γ and χ level off to field-dependent values as $T \to 0$ K. The

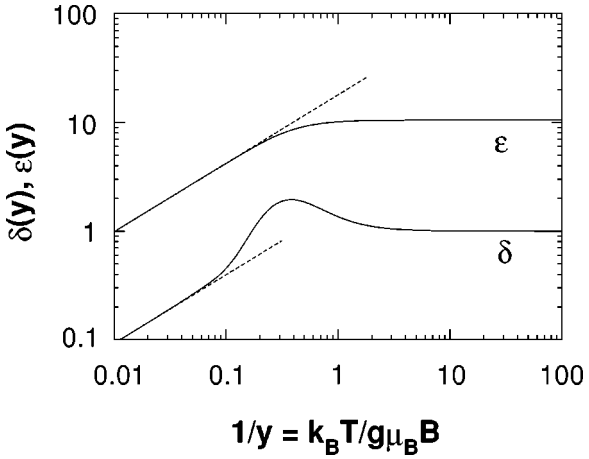

FIG. 1. Plot of the terms $\delta(y)$ and $\varepsilon(y)$ in Eqs. (1) and (2) versus $1/y$. The dashed lines show the asymptotic behavior with $\delta, \varepsilon \sim y^{-\alpha}$.

temperature dependence of the localized moment contributions is then identical to that of the itinerant electrons. For small y (low B/T), $\delta \simeq 1$, $\varepsilon \simeq 10.4$, and Eqs. (1) and (2) reduce to the form given by Paalanen *et al.*[5] for the $B=0$ case. Referring to Eqs. (1) and (2), and to Fig. 1, we can summarize the asymptotic behaviors of the specific heat C and susceptibility χ for the localized moments as follows:

$$C \sim T^{1-\alpha}, \quad T[K] \gtrsim 10B[T], \tag{3}$$

$$C \sim (B^{-\alpha})T, \quad T[K] \lesssim 0.1B[T], \tag{4}$$

$$\chi \sim T^{-\alpha}, \quad T[K] \gtrsim 3B[T], \tag{5}$$

$$\chi \sim B^{-\alpha}, \quad T[K] \lesssim 0.25B[T]. \tag{6}$$

Apart from the behavior given in Eq. (4), the other asymptotic forms above have been observed[2,4,5,7] in the specific-heat and susceptibility data. The form given in Eq. (4) is tested in this paper by analyzing the specific-heat data in nonzero magnetic fields at sufficiently low temperatures. At higher temperatures Eq. (1) is used to analyze available experimental results.

It should be noted that the two-fluid-model equations shown in Eqs. (1) and (2) do not explicitly take into account the possibility of an upper bound to the exchange coupling between spin pairs. If a maximum exchange coupling J_0 is considered, then these equations are valid only for $k_B T \ll J_0$ and $g\mu_B B \ll J_0$.

The inclusion of a maximum exchange coupling into the model makes the localized moment contribution in Eqs. (1) and (2) less convenient to work with, and also introduces an extra parameter J_0. Our numerical analysis shows that we can ignore J_0, and use the shown two-fluid equations, when the following conditions are satisfied:

$$B[T] \lesssim \tfrac{1}{10} J_0[K], \tag{7}$$

$$T[K] \lesssim \tfrac{1}{10} J_0[K]. \tag{8}$$

So the range of temperatures over which the two-fluid equations are found to be valid can provide us with an indication of the range of magnitudes of exchange couplings between the localized moments. This maximum exchange coupling, however, has been quoted[4,5] as being sufficiently large (~ 100 K) so that we can ignore it at the temperatures of interest ($T \lesssim 1$ K), and use the equations as given above.

In applying Eqs. (1) and (2) it is desirable to use the Wilson ratio $(\chi/\chi_0)/(\gamma/\gamma_0)$ for a range of magnetic fields and temperatures.[2] This ratio leads to a cancellation of a number of quantities in the equations which cannot be calculated reliably. However, there do not appear to be C and χ data available for a given set of samples which would permit this to be done. We therefore consider C and χ separately.

It is convenient to write the total magnetic susceptibility as

$$\chi(T) = \chi^* + \zeta \varepsilon(y) T^{-\alpha}, \tag{9}$$

where ζ is a constant and χ^* is the diamagnetic susceptibility of the sample plus the contribution due to itinerant electrons. The contributions to χ^* are temperature independent to a good approximation and give a constant background susceptibility on which the T-dependent localized moment contribution is superimposed.

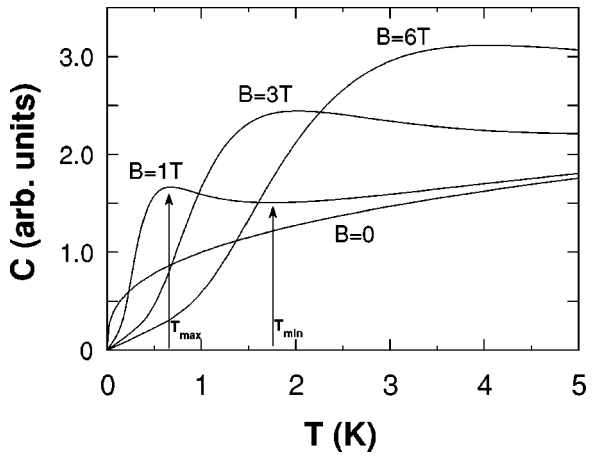

FIG. 2. Specific-heat curves produced by Eq. (11), using a value of $\alpha = 0.65$, for several magnetic field values. $T_{\min}$ and $T_{\max}$ indicate the temperatures at which the local minimum and maximum occur.

For the total specific heat, we may use the expression

$$C(T) = \gamma_i T + \xi \delta(y) T^{1-\alpha} + \beta T^3, \tag{10}$$

where γ_i is the itinerant electron specific-heat coefficient and βT^3 gives the phonon contribution at low temperatures. (For silicon we have a Debye temperature[5] $\Theta_D \simeq 640$ K, corresponding to a value of $\beta = 0.265$ μJ/gK^3.) As with ζ in Eq. (9), ξ is a constant involving the parameter T_0 which, in turn, is linked to the number of localized moments.

The localized moment contribution to the specific heat,

$$C = \xi \delta(y) T^{1-\alpha}, \tag{11}$$

produces a Schottky-type peak in a magnetic field, with asymptotic behaviors given by Eqs. (3) and (4). This is evident from the behavior of the term $\delta(y)$ shown in Fig. 1. In Fig. 2 we show examples of the curves produced by Eq. (11), and show how the specific heat evolves in a magnetic field. A Schottky peak for noninteracting spins is described by the equation $B/T_{\max} \simeq 1.8$, where $T_{\max}$ is the position of the peak in a magnetic field B. The height of a Schottky peak is independent of B, whereas for Eq. (11) the ratio of the specific-heat peak values is described by the simple formula

$$\left(\frac{C_1}{C_2}\right) = \left(\frac{B_1}{B_2}\right)^{1-\alpha}, \tag{12}$$

where C_1 and C_2 are the peak amplitudes for the magnetic fields B_1 and B_2, respectively. For $\alpha < 1$, we therefore observe that the peak amplitude of the specific heat increases as a function of the applied magnetic field, as observed in Fig. 2. It should be noted that the above expression is, however, only valid for values $\alpha > 0.580$. As α is reduced, the quantity $T_{\min}$, defined in Fig. 2, decreases while $T_{\max}$ increases. When $\alpha \simeq 0.580$, $T_{\min} = T_{\max}$, and we only have a point of inflection in the specific-heat curves. For lower values of α, Eq. (11) does not have any local maxima or minima, and the specific heat is then a strictly increasing function of T.

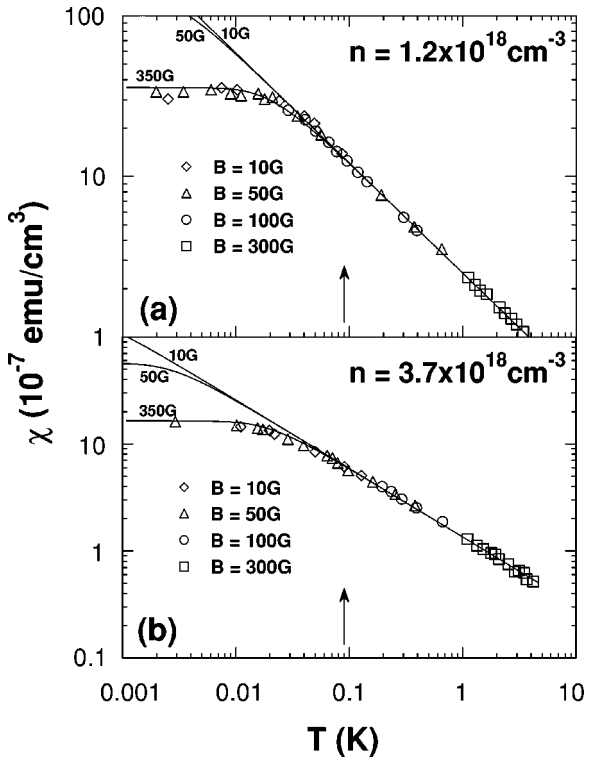

FIG. 3. Susceptibility data (Ref. 8) for two insulating samples. The curves are fits of Eq. (9), with $\chi^*=0$. The arrows indicate the predicted temperature, obtained from Eq. (5), at which the data for all the magnetic field values should converge and follow a $T^{-\alpha}$ form.

III. THE MAGNETIC SUSCEPTIBILITY

The analysis of magnetic susceptibility data using Eq. (9) is comparatively straightforward for insulating and just-metallic cases. Previous work using the scaling approach[4] has suggested that the parameter α, which determines the renormalized J distribution, decreases from values around 0.9 for $n/n_c \lesssim 0.05$ to a plateau value around 0.6 for $n/n_c \lesssim 1$. We have carried out an analysis of the low magnetic field susceptibility data of Andres *et al.*[8] on the insulating side of the transition using Eq. (9) and confirm this behavior for α. These values of α are shown in Fig. 7, together with the values obtained by other researchers, and the values obtained from our specific-heat analysis described below. Figures 3(a) and 3(b) show representative fits to two sets of susceptibility data.

The curves through the data points are fits of Eq. (9), with $\chi^*=0$, since the constant background susceptibility has been subtracted from the data. For each concentration we have varied the value of B from 10 to 350 G. Surprisingly, the curves corresponding to $B=350$ G fit all the data well on the whole temperature range, even though this field value is larger than that specified for the data points. The curves with the proper field values cannot explain the observed low-T saturation in the data below 10 mK. The reason for this discrepancy is not yet clear. The arrows in the figures indicate the temperature at which the curves for this range of fields will converge together, and then follow the $T^{-\alpha}$ behavior. This temperature is obtained from Eq. (5), and the data appear to follow this prediction. All the above features are also present in the other concentrations of the Andres *et al.*[8] data.

Equation (9) has also been successfully applied to χ data obtained in higher applied magnetic fields. Our results for a just-metallic sample have been presented previously[2] using data obtained at temperatures down to 50 mK and in fields up to 1 T. The asymptotic behavior described above is substantiated and the agreement between the prediction of Eq. (9) and experiment is gratifying. In general, the model gives a satisfactory description of the susceptibility data. A more stringent test of the model requires the successful description of specific-heat data, where many questions still remain unanswered. Available experimental results are discussed below.

IV. THE SPECIFIC HEAT

The analysis and description of the specific heat of Si:P are challenging and important aspects in describing this metal-insulator system. Our analysis suggests that great care must be taken in determining the electronic contributions to the specific heat in order to obtain consistent and satisfactory results. We first discuss the specific heat in zero magnetic fields, followed by an analysis of the specific heat in the presence of magnetic fields. Finally, in this section we consider the effects of the nuclear contribution to the specific heat, which is non-negligible at sufficiently low temperatures ($T \lesssim 100$ mK). This contribution is obviously present in large magnetic fields due to the nuclear Zeeman splitting,[7] but we also discuss the possibility of a detectable nuclear contribution even in zero magnetic fields.

A. The specific heat for $B=0$

Previous attempts[6,9] to describe the zero-field specific heat of Si:P for $n \sim n_c$ at fairly low temperatures used the observation that at somewhat higher temperatures ($T \gtrsim 2$ K) the specific heat C appeared to have linear and cubic terms, attributed to the itinerant electron ($\gamma_i T$) and phonon (βT^3) contributions, respectively. Figure 4 shows a representative C/T versus T^2 plot of the total specific heat[6] of Si:P for $n/n_c \simeq 0.45$ ($n_c \simeq 3.52\times10^{18}$ cm^{-3}),[10] which exhibits this behavior. The apparent linear form at higher temperatures can be noticed, with the dashed curve being a fit through these points. The intercept and slope of this curve provide the coefficients γ_i and β, respectively.

The excess specific heat $\Delta C = C - \gamma_i T - \beta T^3$, shown in the inset of Fig. 4, is then attributed to localized moments present in the system. The dashed line indicates the power-law behavior ($\Delta C \sim T^{1-\alpha}$) visible up to temperatures of about 0.4 K. This form is predicted by the Bhatt-Lee model,[3,5] and is contained in Eq. (11) for the case $y=0$.

Several problems can arise, however, when analyzing the zero-field specific heat with the above method. The γ_i values, obtained from the intercepts of linear fits such as those shown in Fig. 4, have been determined as a function of the dopant concentration n. Thomas *et al.*[9] carried out this type of analysis and attempted to show a correspondence between the absolute zero conductivity σ_0 of Si:P and the specific-heat coefficient γ_i. This relationship was not established. Similar results for γ_i have been presented by Kobayashi *et al.*[11] and also Lakner *et al.*[6] for analysis of specific-heat data

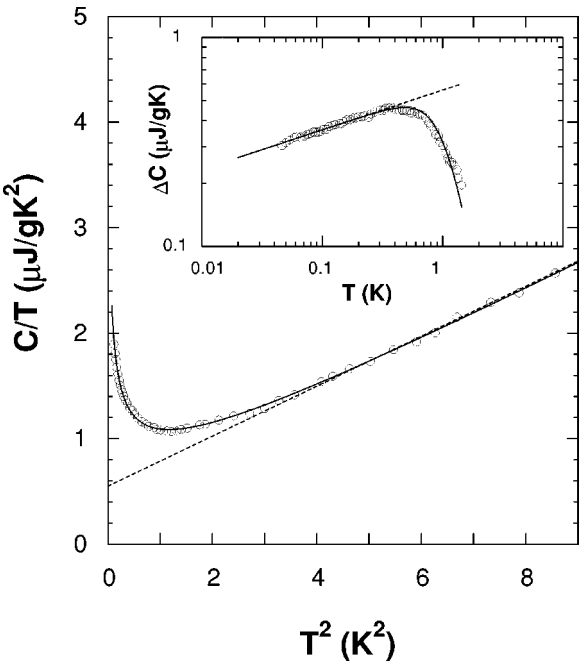

FIG. 4. Specific-heat data (Ref. 6) for $n=1.6\times10^{18}$ cm^{-3} in a C/T versus T^2 plot. The dashed line represents the linear expression $C/T=\gamma_i+\beta(T^2)$ fitted to the higher-temperature points, and the inset shows the excess specific heat $\Delta C=C-\gamma_i T-\beta T^3$ resulting from this fit. The dashed line in the inset shows the power-law form observed at the lower temperatures, while the solid curve is a fit of the model using a maximum exchange coupling of $J_0=3$ K. The solid curve in the main figure is a fit of the expression $C=\xi T^{1-\alpha}+\beta T^3$, and gives a good description of the data on the whole range shown. The implications of these fits are discussed in the text.

in nonzero and zero magnetic fields, respectively. In all cases γ_i was found to have a significant contribution even deep into the insulating phase. It is important to establish whether these values are physically meaningful.

Further inconsistencies arise when analyzing the excess specific heat ΔC. Lakner *et al.*[6] obtained the parameter α as a function of n, which is determined from the slope of the data in a logarithmic plot of ΔC versus T, as in Fig. 4 (inset). The values for α which they found close to the MI transition are larger than those of other earlier studies. Paalanen *et al.*'s[5] analysis of the zero-field specific-heat data produced values of $\alpha\sim0.6$ for $n\sim n_c$, which also corresponds well to the value for α determined from susceptibility analysis.[4] The analysis by Lakner *et al.*, however, produced values of $\alpha\geqslant0.8$.

The rapid decrease in ΔC for $T\gtrsim0.4$ K has been attributed[12] to a cutoff of the cluster excitation energies. If we do consider a maximum exchange coupling J_0 in our formalism, we can reproduce this rapid decrease. The solid curve in Fig. 4 (inset) shows the theoretical prediction using a value of $J_0=3$ K, which is much lower than expected. For the values of $J_0\gtrsim100$ K mentioned in the literature,[4,5] we would, according to Eq. (8), expect the power-law form for ΔC up to at least $T\sim10$ K.

We suggest that the discrepancies above arise from the use of the C/T versus T^2 plot to extract the itinerant contribution γ_i from the limited range of the higher-temperature data points. The γ_i value obtained in this way is at best an upper bound to the true itinerant contribution. By forcing the linear fit in Fig. 4 through the higher-T data points, we minimize the excess specific heat, and force ΔC to vanish as rapidly as possible, as seen in the inset of Fig. 4. If the localized moment contribution does indeed still have a significant contribution at higher temperatures, as we suggest, the above method will certainly produce questionable results.

To emphasize the possible uncertainty in the above procedure, we have found that we can describe the total specific heat in Fig. 4 solely in terms of a localized moment and phonon contribution. The solid curve is a good fit of the expression $C=\xi T^{1-\alpha}+\beta T^3$, and there is no need to introduce an itinerant contribution.

Based on these observations, we have analyzed the zero-field data differently without relying on the above method to obtain γ_i and β. Instead, a direct fit of Eq. (10) was made to the specific-heat data, which for $B=0$ reduces to the simple form

$$C(T)=\gamma_i T+\xi T^{1-\alpha}+\beta T^3, \tag{13}$$

where γ_i, ξ, α, and β are temperature-independent constants for a particular sample, which can be determined from a fit to the total specific-heat data. We note that α and β are constrained somewhat, and the fits depend primarily on γ_i and ξ. For the phonon contribution βT^3, it is possible to use the quoted Debye temperature to determine β. However, Lakner *et al.*,[6] whose data we used for this analysis, state that their thermometry at the higher temperatures was not very accurate and brought about small variations in their determination of Θ_D from the data.

Figures 5(a) and 5(b) show zero-field specific-heat data,[6] together with fits of Eq. (13). We carried out least-mean-square fits of this expression for temperatures $T\geqslant200$ mK. The parameter values were sensitive on the fitting range used. For several samples we found, however, that the parameter values varied rapidly when the lower bound of the fitting range was below and around 100 mK, and were less sensitive when the lower bound was varied above 100 mK. The observed behavior would be consistent with having a small upturn in the data as the temperature is reduced below 100 mK, which can be observed in some of the data. We therefore choose 200 mK as the lower bound to the fitting range to avoid this possible anomaly. This slight upturn at the lowest temperatures may be an experimental artifact. Thermal decoupling effects have been seen on electrical conductivity measurements at the lowest temperatures.[19]

Figures 6(a) and 6(b) show plots of the excess specific heat $\Delta C=C-\gamma_i T-\beta T^3$ which is obtained. Figure 6(a) shows ΔC for three concentrations in the insulating phase, for which $\gamma_i=0$. The electronic specific heat has a power-law form over a larger temperature range than the data shown in Fig. 4 (inset). Figure 6(b) shows ΔC for concentrations just below and above the MI transition for which we obtained nonzero itinerant contributions ($\gamma_i\neq0$). These data also exhibit the power-law component $\xi T^{1-\alpha}$ over almost the whole fitting range.

For the $n=7.3\times10^{18}$ cm^{-3} data, we have no localized moment contribution present ($\xi\sim0$), and this is consistent with Fermi-liquid behavior for $n/n_c\gtrsim2$. From the corresponding γ_i value obtained, we calculate an effective mass

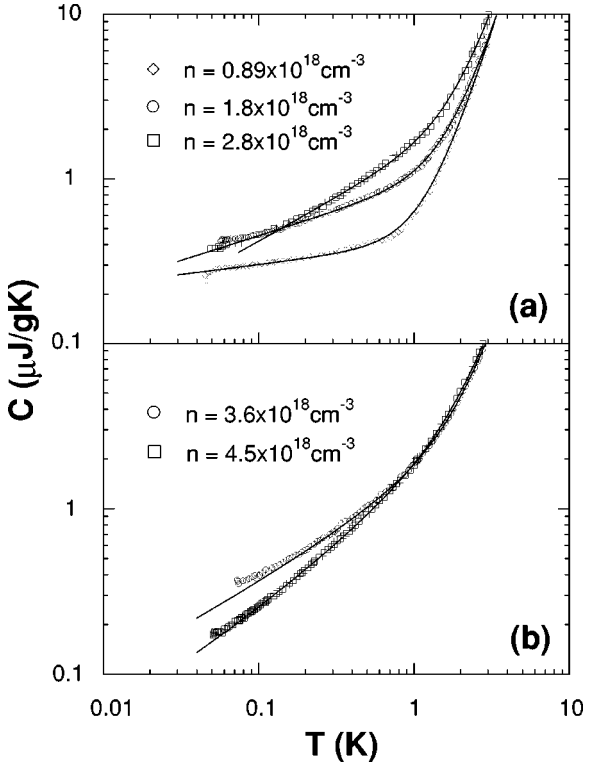

FIG. 5. (a) shows zero-field specific-heat data (Ref. 6) for three insulating samples, while (b) shows data for two metallic samples. The curves are fits of Eq. (13). No itinerant contribution ($\gamma_i=0$) is used for the fits to the insulating samples in (a).

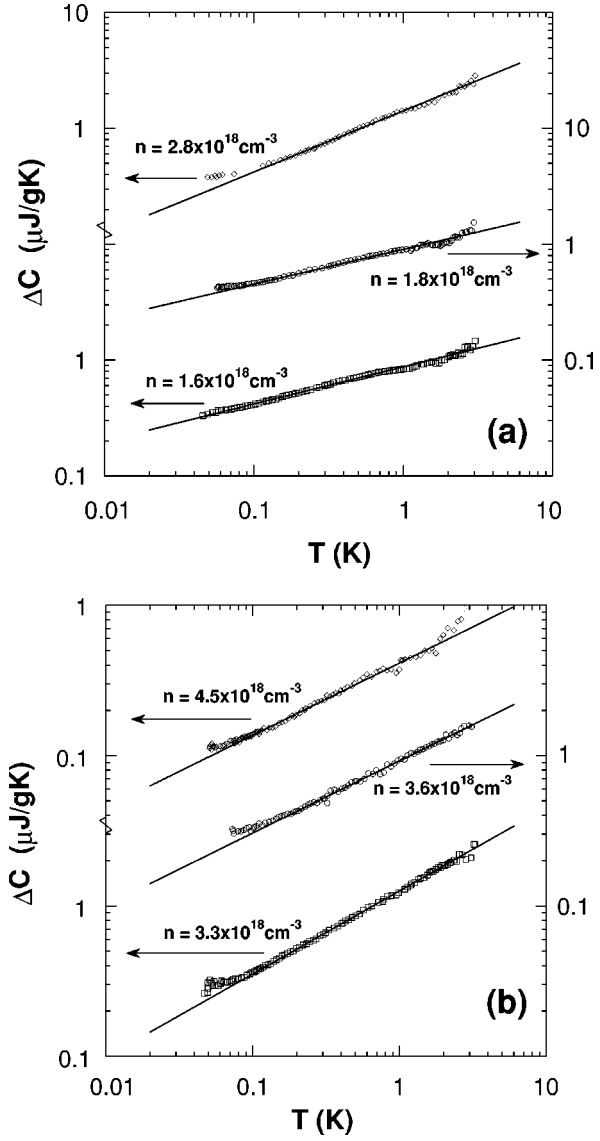

FIG. 6. (a) shows the electronic specific heat $C-\beta T^3$ for three insulating samples. The power-law form $C\sim T^{1-\alpha}$ appears on a larger T range than shown in Fig. 4 (inset). (b) shows the localized moment contribution $\Delta C=C-\gamma_i T-\beta T^3$ for a just-insulating and two metallic samples. Here we again see a power-law form for almost the whole temperature range.

for the impurity electrons as $m^*/m_0^*\simeq 1.2$, which shows a mass enhancement over the Si conduction band mass m_0^*. This value is slightly lower than that predicted by Paalanen *et al.*[5] ($m^*/m_0^*=1.3$), and larger than the value of 1.06 quoted by Harrison and Marko.[13]

Figures 7(a)–7(c) show the results obtained for the parameters α, ξ, and γ_i, respectively, plotted against n/n_c. From the values of β obtained, we have a range of Debye temperatures $\Theta_D\in(625, 685\ \mathrm{K})$.

The values of α obtained, shown in Fig. 7(a), are compared to those obtained from previous susceptibility analysis.[4,8,14–16] For $n/n_c>0.4$, we obtained values of $\alpha\in(0.45,0.7)$ and, except possibly for $n/n_c\sim 0.80$, the values are close to the susceptibility values. This is in contrast to the larger values of $\alpha>0.8$ obtained by Lakner *et al.*[6] As $n\to 0$, we see an increase in α, and a crossing of $\alpha=1$, as also observed by Lakner *et al.* Our formalism of the two-fluid model, involving the renormalized exchange coupling between spins, does not allow for values $\alpha\geqslant 1$. We do expect that $\alpha\to 1$ as n decreases well below n_c, corresponding to a system of isolated spins. This increase of α towards 1 with decreasing n is also observed in the susceptibility. We suggest that there could be a low-temperature anomaly in the specific-heat measurements which at the low concentrations may lead to inflated values of α. Furthermore, the analysis in Sec. IV B of the specific heat in magnetic fields points to the possibility of an excess specific-heat contribution. To demonstrate this possibility, we have compared the specific-heat data of Lakner *et al.*[6] and Harrison and Marko.[13]

Figure 8 shows two sets of specific-heat data for insulating samples. The curves through the Harrison and Marko data (■ and ●) are fits of the expression $C=\xi T^{1-\alpha}+\beta T^3$, with $\beta=0.265\ \ \mu\mathrm{J/gK}^4$ ($\theta_D=640$ K). The fits to both sets of data are satisfactory, although the value of $\alpha=0.44$ obtained for the high concentration is lower than expected. The main point, however, is the comparison between the two sets of data for the low concentration. The value of $\alpha=0.89$ obtained is very close to the susceptibility values shown in Fig. 7, and there is clearly no upturn as observed in the Lakner *et al.* data, which produces a value of $\alpha>1$. Further experiments would be helpful in clarifying this apparent discrepancy.

The localized moment contribution ξ, shown in Fig. 7(b), steadily increases from zero as n is increased, and near the MI transition starts to decrease towards zero, vanishing at $n/n_c\simeq 2$. It is expected[5,9,17] that the Si:P system should show Fermi-liquid behavior for $n/n_c\gtrsim 2$, which appears to be the

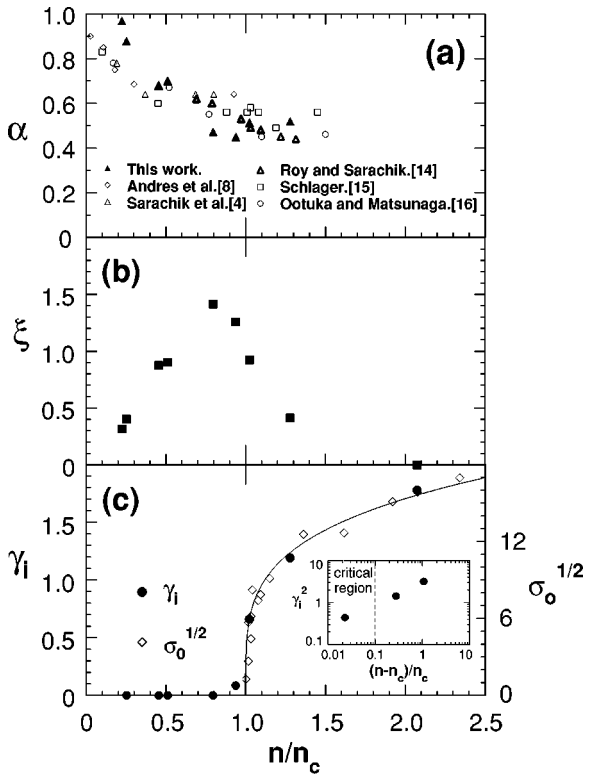

FIG. 7. (a)–(c) show the results obtained by fitting Eq. (13) to zero-field specific-heat data. (a) plots the parameter α versus n/n_c, and these values are compared to previous α values obtained from susceptibility analysis. (b) and (c) show the results for ξ and γ_i, respectively. Also included in (c) is data (Ref. 18) for the absolute zero conductivity σ_0 for comparison. The inset of (c) shows γ_i^2 versus $(n-n_c)/n_c$ for the metallic phase in a logarithmic scale.

case here with the vanishing localized moment contribution. Overall, the behavior of ξ is as expected.

The itinerant contribution values γ_i shown in Fig. 7(c) are, however, different from those obtained previously,[6,11] which decrease gradually through the MI transition as n is decreased, and have a significant contribution even deep into the insulating phase. In contrast, the γ_i values obtained here decrease more rapidly through the MI transition, and vanish in the insulating phase for $n/n_c \lesssim 0.8$. Convergence between the previous and the present γ_i values only occurs in the metallic phase when the localized moment contribution vanishes.

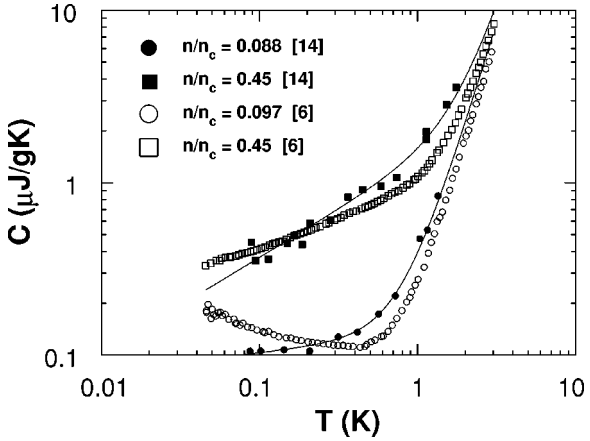

FIG. 8. Comparison of the specific-heat data from two different sources (Refs. 6,13) for two insulating samples. The curves are fits of the equation $C=\xi T^{1-\alpha}+\beta T^3$ to the Harrison and Marko (Ref. 13) data.

It should be noted that the data for the just-insulating sample ($n/n_c=0.94$) can also be accurately described in terms of only a localized moment contribution, with a slightly smaller value of $\alpha=0.43$. The nonzero γ_i value for this sample was produced by the fitting routine, but it is possible that $\gamma_i=0$ for all the insulating samples.

In Fig. 7(c) we have also included data[18] for the absolute zero conductivity σ_0 for comparison. We plotted $\sqrt{\sigma_0}$ in view of the attempt by Thomas *et al.*[9] to relate γ_i^2 and σ_0. The curve represents the expression $\sigma_0=235(n/n_c-1)^{\mu}$, with $\mu=0.5$ the critical exponent for Si:P,[18] and even appears to describe the form of γ_i in the metallic phase. There appears, therefore, to be a possible scaling between γ_i^2 and σ_0, as proposed by Thomas *et al.* More metallic phase data are required to substantiate this relationship.

Recent analysis,[19,20] however, has reopened the question of the value of μ in Si:P, but we choose $\mu=0.5$ for consistency with the previous analysis based on a particular value of n_c. There is evidence[19,20] that $\mu\approx 1$ for just-metallic samples with $(n-n_c)/n_c \lesssim 0.1$. The inset of Fig. 7(c) shows a plot of γ_i^2 versus $(n-n_c)/n_c$, and indicates the critical region[19] close to the MIT where it is predicted that $\mu\approx 1$. If γ_i^2 and σ_0 do scale, then we would expect that $\gamma_i^2 \sim (n/n_c-1)^{\mu}$, with $\mu\approx 1$ in this critical region. We do not, however, have sufficient data to confirm this behavior. The two data points outside of the critical region produce a slope of 0.67, close to the value of $\mu=0.64$ obtained by Stupp *et al.*[19] from their conductivity data in this region.

The major feature of our results is that for $n/n_c \lesssim 0.8$ the data do not have an itinerant contribution ($\gamma_i=0$), and the electronic specific heat in the insulating phase can be described using only the Bhatt-Lee model. We also find that the power-law form $T^{1-\alpha}$ is present over the whole fitting range. From Eq. (8) we can therefore estimate that $J_0>30$ K. For $n<1\times 10^{18}$ cm^{-3}, the results are not as satisfactory. An explanation for the anomalous behavior in the specific heat at the lower temperatures, as observed in Fig. 8, is required.

B. Specific heat in a magnetic field

In the presence of finite magnetic fields, the specific heat of Si:P develops Schottky-type peaks.[6,11] Previous attempts to describe these data used the Schottky expression $C_{\rm sch}$ for the localized moment contribution, introducing an effective magnetic field $B_{\rm eff}$ and an effective concentration $n_{\rm eff}$ of localized moments to fit the data.[21] The total specific heat is then modeled by the equation

$$C=C_{\rm sch}+\gamma_i T+\beta T^3. \tag{14}$$

The excess specific heat $\Delta C=C-\gamma_i T-\beta T^3$, obtained from these fits of Eq. (14) to the total specific-heat data, cannot then be described by Eq. (11). The excess specific heat obtained in this way is, however, not adequate in testing models which consider electron-electron interaction. The fitting parameters are chosen in such a way that ΔC matches

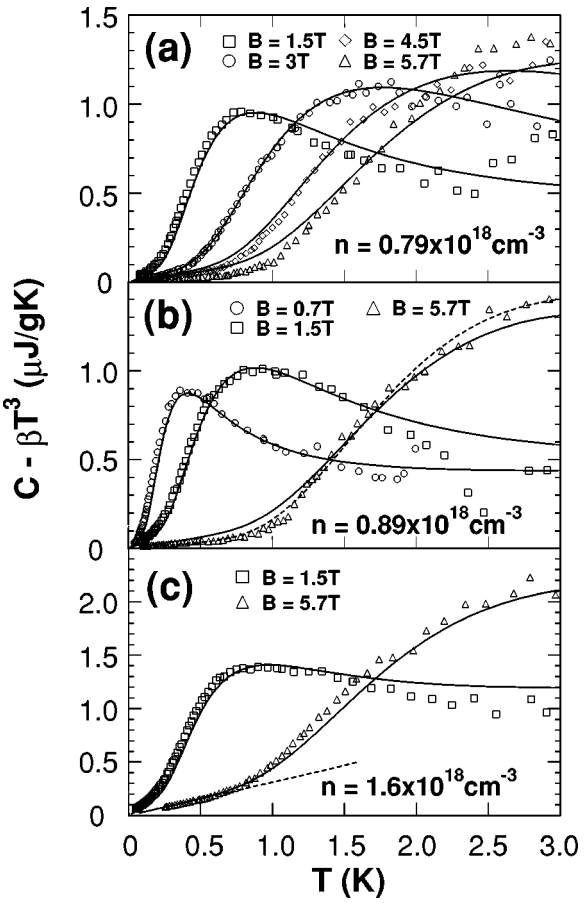

FIG. 9. (a)–(c) show the electronic specific heat (Ref. 6) $C-\beta T^3$ for three insulating samples ($n/n_c \simeq 0.22$, $n/n_c \simeq 0.25$, and $n/n_c \simeq 0.45$, respectively) in various magnetic fields. The curves are fits of Eq. (11). For each concentration only the field value B is varied.

$C_{\rm sch}$ as closely as possible. This in part explains why our earlier attempts to describe this excess specific heat in terms of a Herring-Flicker coupled spin-pair system[22] also failed for $n/n_c \gtrsim 0.2$. Instead, our analysis proceeds to explain the total specific-heat data by comparison to the theoretical prediction in Eq. (10).

Figures 9(a)–9(c) show the electronic specific heat $C-\beta T^3$ in various magnetic fields for three insulating samples $n/n_c \simeq 0.22$, 0.25, and 0.45, respectively. For the phonon contribution βT^3, we used the β values obtained from our analysis of the corresponding zero-field specific-heat data, as described in the previous subsection. The curves are fits of Eq. (11) which describes the localized moment contribution to the specific heat in the two-fluid model. As for the zero-field specific heat, we do not need to introduce an itinerant contribution $\gamma_i T$ to give a satisfactory description of the data in nonzero fields.

For the two lower concentrations ($n/n_c \simeq 0.22$ and 0.25), we determined α from the evolution of the peak amplitude in the magnetic field. Using Eq. (12), which describes this peak amplitude evolution, we can estimate that $\alpha \sim 0.8$ for both these concentrations. This value of α is lower than the value obtained from the zero-field data, but is very close to the values obtained from susceptibility studies, as indicated in Fig. 7(a). The only fitting parameter is therefore ξ, which can be easily determined by matching the peak amplitudes of the curves and the data. For the $n/n_c \simeq 0.45$ data in Fig. 9(c), we cannot use Eq. (12) to determine α, since we only have one well-defined peak. For these data we find that the zero-field value of $\alpha \sim 0.68$ gives a good description.

It should be noted that we fixed α and ξ for each concentration, and only varied the magnetic field B to generate the family of curves in the plots. The large scattering in the high-temperature data points could be attributed to the loss in thermometry accuracy,[6] and could also be responsible for the unusual high-temperature ($T > 1.5$ K) deviation of the $B = 1.5$ T data in Fig. 9(b). In general, the predictions of the model give a gratifying description of the data, particularly for the lower field values ($B < 5.7$ T). Clearly, much better fits to the data can be obtained by allowing α, ξ, and β to vary for each set.

For the two lower concentrations in Figs. 9(a) and 9(b), we observe for the largest field ($B = 5.7$ T) that the curve deviates appreciably from the data for $T \sim 1$ K. This deviation can be corrected by increasing the value of α. To demonstrate this, the dashed curve in Fig. 9(b) shows the change in the predicted behavior when α is increased to a larger value of $\alpha = 0.9$. This behavior at larger field values can be expected. As $\alpha \rightarrow 1$, the system tends towards an isolated spin system, with an increase in α corresponding to a reduction in the effective exchange couplings between the localized moments. A shrinkage in the localized moment wave function caused by a large magnetic field would reduce the exchange couplings, and could explain this increased α value. This effect is not observed in the $n/n_c \simeq 0.45$ data in Fig. 9(c). For this concentration, we have larger exchange couplings (indicated by the smaller value of α), and a noticeable increase in α might only become apparent at even larger fields.

The theory provides a good description of the evolution of the specific heat in a magnetic field. Notice that the peak height increases as B is increased. In using the simple Eq. (14), it is necessary to use a field-dependent effective concentration $n_{\rm eff}$ to account for this peak height increase, which is then attributed to field-induced localization.[7] This is not necessary with the present model since the peak height increases automatically as B is increased, as described by Eq. (12). Just as for the Schottky expression $C_{\rm sch}$, the peak details alone can provide us with both the fitting parameters α and ξ.

The localized moment contributions ξ obtained from the $B \neq 0$ analysis for the above three concentrations are somewhat lower than those values obtained from the $B = 0$ analysis. If we were to fit Eq. (13) to the $B = 0$ data using the $B \neq 0$ parameter values, then we find that the apparent excess specific heat in the data is similar for all three samples, and also similar in magnitude to the anomalous upturn in the $n = 0.34 \times 10^{18}$ cm^{-3} data shown in Fig. 8. This difference in the parameter values from the $B = 0$ and $B \neq 0$ data requires further investigation. This problem does not appear to occur in the higher concentration data, where we can describe both the $B = 0$ and $B \neq 0$ specific-heat data using the same parameter values.

For larger concentrations where it is necessary to introduce a nonzero itinerant contribution $\gamma_i T$, the specific heat

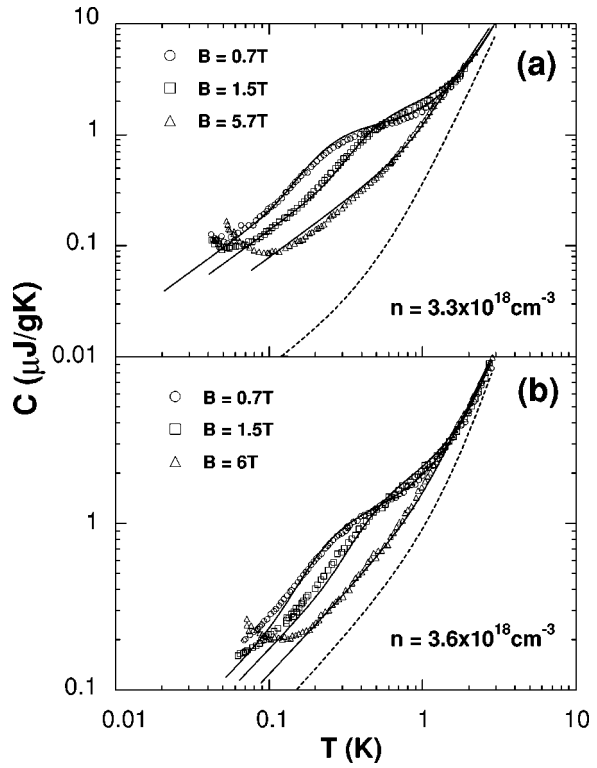

FIG. 10. (a) and (b) show the total specific heat (Ref. 6) for just-insulating ($n/n_c \simeq 0.94$) and just-metallic ($n/n_c \simeq 1.02$) samples. The solid curves are fits of Eq. (10), while the dashed curves show the contribution $\gamma T + \beta T^3$. For each concentration only the field value B is varied.

can still be described by Eq. (10), but the determination of the fitting parameters is more difficult and uncertain. Equation (12) cannot now be used to easily obtain α (and hence ξ) from the peak heights, since the $\gamma_i T$ contribution has to be determined and removed first. Also, as Fig. 7(a) indicates, for concentrations close to and above the MI transition, we have $\alpha < 0.580$, and Eq. (12) cannot be used to determine α, as mentioned in Sec. II.

In Figs. 10(a) and 10(b) we show the total specific heat in nonzero magnetic fields for a just-insulating ($n/n_c \simeq 0.94$) and just-metallic ($n/n_c \simeq 1.02$) sample, respectively. The curves are plots of Eq. (10), with the parameters γ_i, ξ, α, and β equal to the values determined from the $B=0$ specific-heat analysis. For each figure we varied only the magnetic field B, and the curves give a reasonable description of the data and the evolution of the specific heat in a magnetic field. For the $n/n_c \simeq 0.94$ data in Fig. 10(a), we do obtain better fits if we let $\gamma_i = 0$, and, as we mentioned in the previous subsection, it is possible that for this just-insulating sample there is no itinerant contribution.

In Fig. 9(c) we have also shown the asymptotic $T \to 0$ K behavior as specified by Eq. (4), which predicts that ΔC vanishes linearly in T at sufficiently low temperatures, with the slope decreasing with increasing B. This behavior can also be observed in the curves of Figs. 10(a) and 10(b). This predicted behavior appears to be present for all the concentrations, but complete verification of this property is difficult. There is a pronounced upturn in the data for $T < 100$ mK, clearly visible in Figs. 10(a) and 10(b), which is attributed to the nuclear specific heat. In the next subsection we consider the prediction of Eq. (4) in conjunction with this nuclear contribution.

C. The nuclear contribution to the specific heat

We now consider the asymptotic low-T behavior of the specific heat, and also consider the anomalies that occur at temperatures $T \lesssim 100$ mK, attributed to the nuclear Zeeman splitting. The two-fluid model predicts that the localized moment contribution vanishes linearly in T as $T \to 0$ K, as proposed by Eq. (4). Since the itinerant contribution is also linear in T, we predict for the total electronic specific heat

$$C_{\rm elec} = \gamma^* T, \quad T[K] \lesssim 0.1 B[T], \tag{15}$$

where γ^* now includes both the localized and itinerant contributions. As mentioned above, verification of this behavior is made difficult by the appearance of an anomaly at the lowest temperatures. It is likely that the ^{31}P nuclei, and possibly some neighboring ^{29}Si nuclei, give rise to a nuclear Schottky term in the specific heat. We adopt the form

$$C_{\rm nuc} = \frac{\eta}{T^2}, \tag{16}$$

which should be a good approximation to the nuclear specific heat at the temperatures we are dealing with ($T \gtrsim 50$ mK).

For the analysis we use the highest field data, since this should provide the largest temperature interval over which the prediction of Eq. (15) should hold. The anomaly is also most pronounced for higher fields.

The phonon contribution βT^3 is subtracted from the total specific heat, and, combining Eqs. (15) and (16), we have the prediction

$$\frac{C}{T} = \gamma^* + \frac{\eta}{T^3}, \quad T[K] \lesssim 0.1 B[T], \tag{17}$$

with γ^* and η as fitting parameters. The parameter η will give us an indication as to the concentration of nuclei contributing to the anomaly.

Figures 11(a)–11(c) show the results for three metallic samples. For the concentration $n = 7.3 \times 10^{18}$ cm^{-3} shown in Fig. 11(a), Eq. (17) is expected to hold for all temperatures since the localized moment contribution is negligible. In Figs. 11(b) and 11(c) the arrow indicates the temperature below which we predict Eq. (17) to hold. For all three concentrations, the prediction gives a good account of the data, and supports the idea that the upturn is due to the nuclei. The asymptotic prediction in Eq. (4) is also supported here. The magnitude of η indicates a concentration of nuclei of the order of the dopant concentration. This is consistent with previous statements[7] that it is mainly the ^{31}P nuclei that contribute to the specific heat, with the majority of the ^{29}Si nuclei having spin-lattice relaxation times which are so long that their contribution is not seen on the time scale of the experiments.

Results for insulating samples are not as convincing, although the general behavior is consistent with the predictions of Eq. (17). On the insulating and just-metallic sides of the transition the ^{31}P nuclei associated with the localized electrons may experience effects due to the hyperfine coupling as

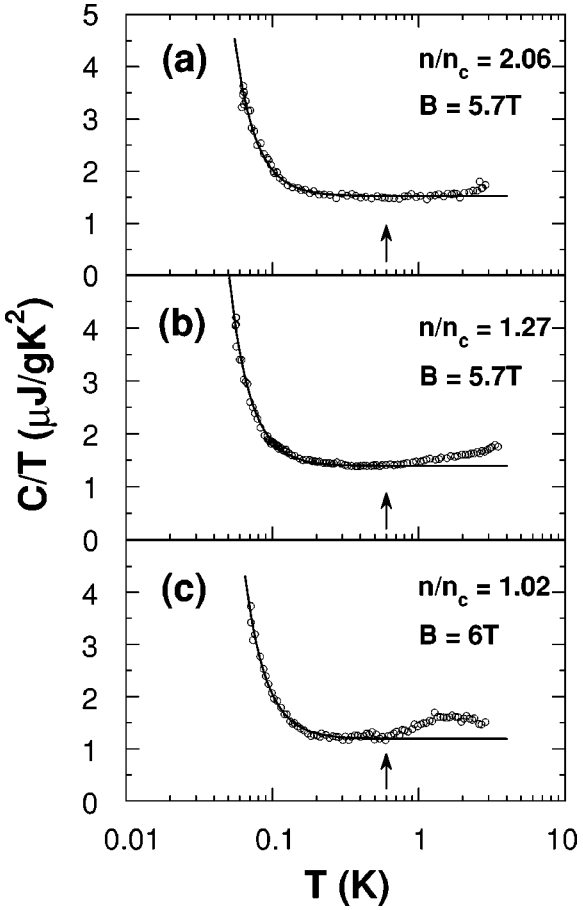

FIG. 11. Specific-heat data (Ref. 6), $C-\beta T^3$ in a large magnetic field for three metallic samples. The data are shown in a C/T versus T plot to test the predictions of Eq. (17). The arrow indicates the temperature below which this expression is expected to be valid.

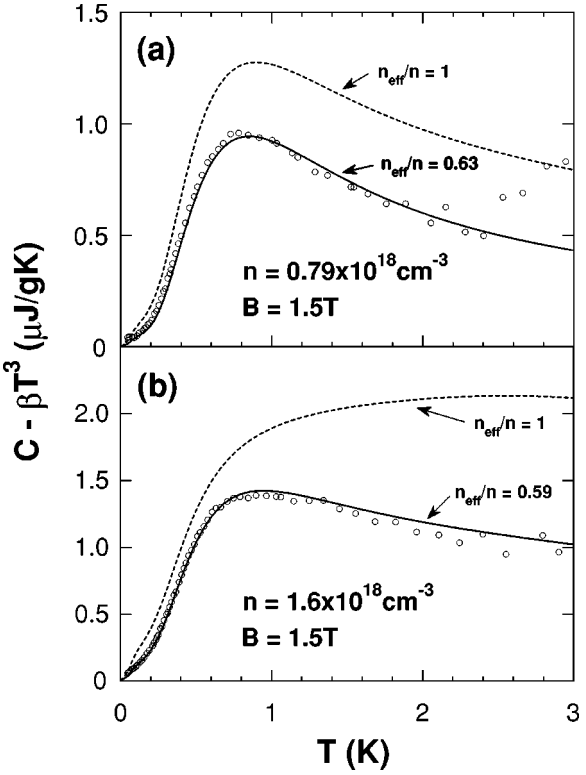

FIG. 12. The electronic specific heat (Ref. 6) $C-\beta T^3$ for two insulating samples in a field $B=1.5$ T, with (a) $n=0.79\times10^{18}$ cm^{-3} and (b) $n=1.6\times10^{18}$ cm^{-3}. The curves are fits of the Herring-Flicker spin-pair model (Ref. 22), with the introduction of a single parameter $n_{\rm eff}/n$.

well as an applied field. The hyperfine coupling for ^{31}P nuclei in Si:P has been quoted as 6.8 T.[17,23] This is larger than the highest field of 6 T used in the specific-heat experiments. Because of the exchange effects and spin-lattice relaxation, some averaging of the hyperfine field will occur on the time scale ($\sim$1 s) (Ref. 6) associated with the specific-heat measurements. Because of polarization of triplet state spin pairs by the external field, hyperfine effects will raise the temperature at which nuclear Schottky effects are seen. The lack of high-field specific-heat data below 50 mK makes it difficult to test these ideas in a quantitative way.

An interesting possibility which needs to be considered is that hyperfine effects could play a role in the zero-field data. If some of the localized moments pair with the triplet (ferromagnetic) state as the ground state, as has been suggested,[24] and have sufficiently long spin-lattice relaxation times ($T_1>1$ s) at the temperatures of interest ($T<100$ mK), then it is quite possible that the associated ^{31}P nuclei could make a contribution to the specific heat even for zero applied field. Such effects could explain the anomalous zero-field specific-heat data mentioned above. Further specific-heat measurements down to much lower temperatures ($T\lesssim10$ mK) would help in testing this suggestion.

V. THE HERRING-FLICKER COUPLED SPIN-PAIR MODEL REVISITED

In a previous publication,[22] we presented results on a spin-pair model with an exchange coupling described by the Herring-Flicker expression. The predictions of this model were compared against specific-heat data, where the localized moment contributions were obtained by the use of Eq. (14). The theoretical curves for the spin-pair specific heat were significantly broader than the given data, which, due to the use of Eq. (14), are described better by the Schottky equation $C_{\rm sch}$. In view of the approach to extract the localized moment contribution given in this paper, we revisited the Herring-Flicker coupled spin-pair model, and the results are shown in Figs. 12(a) and 12(b).

Figures 12(a) and 12(b) show electronic specific-heat data ($C-\beta T^3$) for the concentrations $n/n_c\simeq0.22$ and $n/n_c\simeq0.45$, respectively, both for a magnetic field of $B=1.5$ T. The dashed curves show the predictions of the model, and in both cases overestimate the magnitude of the data. By introducing an effective concentration of spin pairs $n_{\rm eff}$, however, we can get a better description of the data, as shown by the solid curves. This reduction in $n_{\rm eff}/n$ can be attributed to larger cluster formation, with $n_{\rm eff}/n$ decreasing as the donor concentration is increased. So, by introducing a single free parameter $n_{\rm eff}/n$ into this model, we can indeed give a good description of specific-heat data in the presence of a magnetic field. However, this approach, which requires numerical calculations, does not provide the simple analytical ex-

pressions and general predictions of the kind given by the two-fluid model discussed above.

VI. CONCLUSION

Using the two-fluid-model equations, we have analyzed low-temperature thermodynamic data for Si:P for a range of concentrations. The behavior of the extracted localized (ξ) and itinerant (γ_i) contributions with n/n_c are of great importance in giving information which may be used to test other theories. The procedures used in obtaining the ξ and γ behavior from measurements must therefore be subjected to careful scrutiny and tests to ensure that they are as reliable as possible.

In this paper we have introduced an analysis of specific-heat data which has produced some interesting results. The previous inconsistencies in the values for the renormalized exchange coupling distribution parameter α obtained from the susceptibility and specific-heat analysis have been somewhat reduced. There is also evidence to indicate that the low-temperature specific-heat anomaly observed in the low concentration samples may not be intrinsic to the system, and that the model may be applied to even lower concentrations.

We have shown that the two-fluid model can be successfully applied to describe the specific heat in both zero and nonzero magnetic fields, and also gives a satisfactory description of susceptibility data. In addition to the parameter α which describes the renormalized exchange coupling, and lies in a limited range, there are two other parameters in this two-fluid model which essentially provide the concentrations of the fluids. For $n/n_c \lesssim 0.8$, we need not introduce an itinerant electron contribution, with the data being described sufficiently in terms of only localized moments. The possibility remains that this is true for all insulating samples ($n/n_c < 1$). The fits to a substantial body of experimental data which have been obtained by choosing rather few parameters are gratifying.

In conclusion, the two-fluid model provides a good description of the thermodynamic data over a large range of dopant concentrations. For $n/n_c \lesssim 0.8$, the data can be successfully described by using only the localized moment contribution. As $n/n_c \to 0$, we expect a crossover to an isolated spin system, and this is contained in the model by letting $\alpha \to 1$. For $n/n_c \gtrsim 2$, the system behaves as a Fermi liquid, and the data is then described by the itinerant contribution. For $0.8 \lesssim n/n_c \lesssim 2$, both the localized and itinerant components are required for a full description.

Measurements of the Wilson ratio in large magnetic fields would be very useful in further testing this model, and in extracting more accurate physical parameters. Specific-heat measurements down to even lower temperatures ($T \sim 1$ mK) would allow for a more detailed analysis of the nuclear contribution, and could also provide more insight into the electronic properties.

ACKNOWLEDGMENTS

We express our gratitude to Professor H. von Löhneysen for supplying us with specific-heat data used in this analysis, and for his comments on our results. Funding for this research provided by the Foundation for Research Development and the University of the Witwatersrand is gratefully acknowledged.

[1] D. Belitz and T. R. Kirkpatrick, Rev. Mod. Phys. **66**, 261 (1994).
[2] M. J. R. Hoch and C. Kasl, Phys. Rev. B **54**, 1435 (1996).
[3] R. N. Bhatt and P. A. Lee, Phys. Rev. Lett. **48**, 344 (1982).
[4] M. P. Sarachik, A. Roy, M. Turner, M. Levy, D. He, L. L. Isaacs, and R. N. Bhatt, Phys. Rev. B **34**, 387 (1986).
[5] M. A. Paalanen, J. E. Graebner, R. N. Bhatt, and S. Sachdev, Phys. Rev. Lett. **61**, 597 (1988).
[6] M. Lakner, H. von Löhneysen, A. Langenfeld, and P. Wölfle, Phys. Rev. B **50**, 17 064 (1994).
[7] M. Lakner and H. v. Löhneysen, Phys. Rev. Lett. **63**, 648 (1989).
[8] K. Andres, R. N. Bhatt, P. Goalwin, T. M. Rice, and R. E. Walstedt, Phys. Rev. B **24**, 244 (1981).
[9] G. A. Thomas, Y. Ootuka, S. Kobayashi, and W. Sasaki, Phys. Rev. B **24**, 4886 (1981).
[10] M. Lakner and H. v. Löhneysen, Phys. Rev. Lett. **70**, 3475 (1993).
[11] N. Kobayashi, S. Ikehata, S. Kobayashi, and W. Sasaki, Solid State Commun. **32**, 1147 (1979).
[12] H. von Löhneysen, Festkoerperprobleme **30**, 95 (1990).
[13] J. P. Harrison and J. R. Marko, Philos. Mag. **34**, 789 (1976).
[14] A. Roy and M. P. Sarachik, Phys. Rev. B **37**, 5531 (1988).
[15] H. G. Schlager, Dissertation, Shaker-Verlag, Aachen, 1996.
[16] Y. Ootuka and N. Matsunaga, J. Phys. Soc. Jpn. **59**, 1801 (1990).
[17] H. Alloul and P. Dellouve, Phys. Rev. Lett. **59**, 578 (1987).
[18] M. A. Paalanen and R. N. Bhatt, Physica B **169**, 223 (1991).
[19] H. Stupp, M. Hornung, M. Lakner, O. Madel, and H. v. Löhneysen, Phys. Rev. Lett. **71**, 2634 (1993).
[20] I. Shlimak, M. Kaveh, R. Ussyshkin, V. Ginodman, and L. Resnick, Phys. Rev. Lett. **77**, 1103 (1996).
[21] H. von Löhneysen and M. Lakner, Physica B **165-166**, 285 (1990).
[22] M. J. R. Hoch and C. Kasl, Phys. Rev. B **49**, 2331 (1994).
[23] G. Feher, Phys. Rev. **114**, 1219 (1959).
[24] M. Eto and H. Kamimura, Phys. Rev. Lett. **61**, 2790 (1988).